Journal of Modern Optics
Vol. 59, No. 5, 10 March 2012, 460–469

Taylor & Francis
Taylor & Francis Group

Binary spatial amplitude modulation of continuous transverse modal electric field using a single lens for mode selectivity in multimode fiber

Angela Amphawan[a,b]*

[a]*InterNetWorks Research Group, School of Computing, Universiti Utara Malaysia, 06010 Sintok, Malaysia;*
[b]*Department of Engineering Science, University of Oxford, Parks Road, Oxford OX1 3PJ, UK*

(*Received 17 August 2011; final version received 21 October 2011*)

The demand for portable real-time optical applications such as medical optical sensors and optical transceivers instigate the need for compact optical designs. The aim of this paper is to demonstrate a new, compact design for binary spatial amplitude modulation in a mode-selective transmitter in a multimode fiber, adapted from microscopy. Results show that it is possible to retrieve the original continuous-amplitude transverse modal electric field from the binary amplitude-modulated image using a single lens. The retrieved image is in good agreement with the original image.

Keywords: spatial amplitude modulation; mode selectivity; dispersion mitigation; bandwidth enhancement; spatial light modulator

1. Introduction

The demand for portable real-time optical applications such as medical optical sensors [1–4] and optical transceivers [5–8] instigate the need for compact optical designs. The aim of this paper is to demonstrate a new, compact design for binary spatial amplitude modulation in a multimode fiber-based optical transceiver, adapted from a confocal microscope [9]. In [9], the original technique was used for tuning the pupil function of the objective lens in a confocal microscope. The main contribution is to demonstrate that the technique used in a confocal microscope may be modified and used in a different application, namely an optical transceiver in a multimode fiber (MMF). In this paper, the modified binary spatial amplitude modulation scheme is used for mode selectivity in an optical transceiver. Apart from applying the microscopy technique to an optical transceiver, another important contribution is the reduction in the number of Fourier transforms used for retrieving the original image from the binary amplitude-modulated image. In [9], a pair of Fourier transforms was required for the retrieval of the original, image whereas here only one Fourier transform is required. Hence, only a single lens is required instead of a pair of lenses, simplifying the alignment procedure and allowing the reduction of the length of the experimental setup. This is essential in the design of real-time portable optical applications such as optical sensors and optical transceivers. To illustrate the application of the proposed scheme, the continuous-amplitude transverse modal electric field of an optical fiber is used in a mode selectivity experiment in multimode fiber. Results show that the retrieved image is in good agreement with the original image.

The paper is organized as follows. In Section 2, the mathematical derivation for the new technique is given. Section 3 describes the simulation of the binary amplitude-modulated signals. Section 4 presents an experimental demonstration of the new binary spatial amplitude modulation technique for mode selectivity in optical fiber communications. Finally, Section 5 provides verification for the new modulation.

2. Mathematical derivation

The new binary spatial amplitude modulation technique is adapted from a microscopy technique for tuning the pupil function of the objective lens in a confocal microscope proposed by Neil et al. [9]. The main contribution is the reduction in the number of Fourier transforms used for retrieving the original image from the binary amplitude-modulated image. In [9], a pair of Fourier transforms was required for the retrieval of the original image. In this work, only one Fourier transform is required. The experimental setup for generating the modal electric field is shown in Figure 1. A 128×128 pixel transmissive binary amplitude spatial light modulator (SLM) supplied by CRL Smectic Technology was used. A summary of the

*Email: angela@uum.edu.my

ISSN 0950–0340 print/ISSN 1362–3044 online

http://dx.doi.org/10.1080/09500340.2011.636486
http://www.tandfonline.com

technique used for generating the modal electric field is given in Figure 2.

The transverse electric field for the LP_{lm} mode of a weakly-guiding infinite parabolic MMF, $\mathbf{e}_{lm}$, is composed of two orthogonal polarizations:

$$b(x, y) = F \sin l\phi, \tag{1}$$

$$b(x, y) = F \cos l\phi. \tag{2}$$

$F(x, y)$ is the radial dependence of the transverse electric field, given by [10]:

$$F(x, y) = R^l L_{m-1}^{(l)}(VR^2) \exp(-0.5VR^2), \tag{3}$$

where R is the normalized core radius, ϕ is the azimuthal angle in the plane of the MMF core, V is the normalized frequency, $L_{m-1}^{(l)}$ is the generalized Laguerre polynomial, l is the azimuthal mode number and m is the radial mode number.

First, the Fourier transform of any polarization of the transverse modal electric field in Equation (1) or Equation (2) is taken. This yields:

$$d(x, y) = \mathcal{F}[b(x, y)]. \tag{4}$$

where $\mathcal{F}$ is the Fourier transform operator.

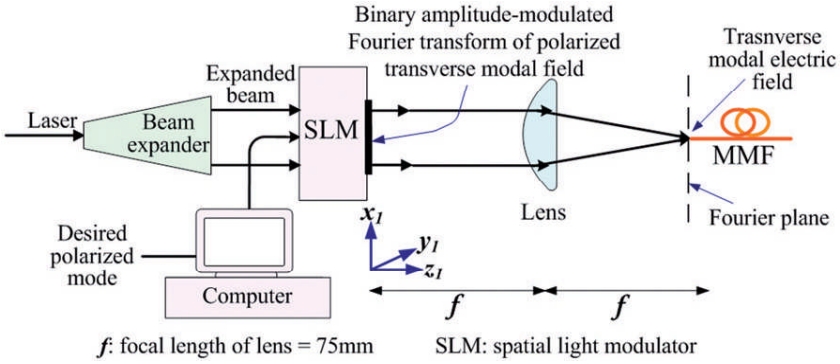

Figure 1. Experimental setup for holographic selective mode excitation. (The color version of this figure is included in the online version of the journal.)

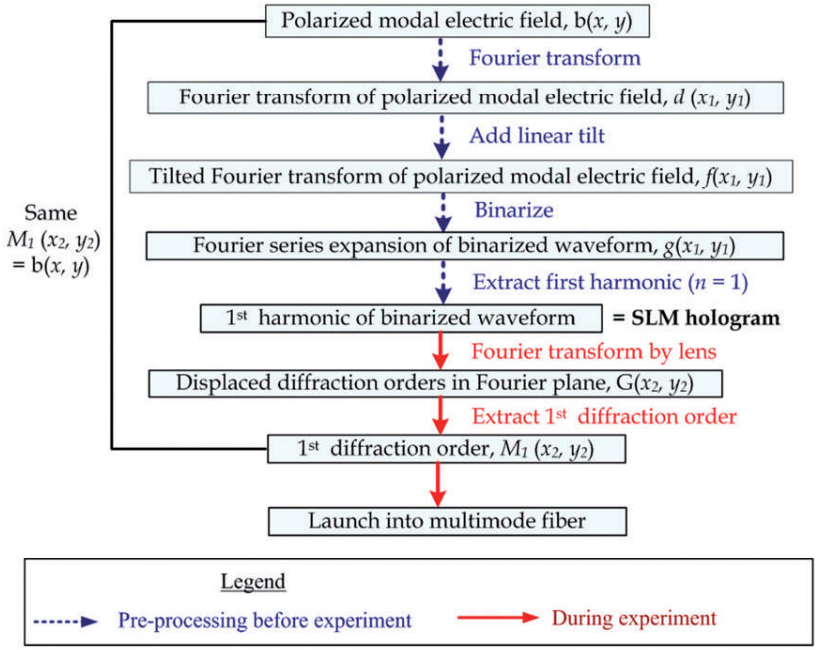

Figure 2. Summary of technique used for generation of modal electric field. (The color version of this figure is included in the online version of the journal.)

Then, a linear tilt is added to the Fourier transformed field. This yields the complex field:

$$f(x_1, y_1) = d(x_1, y_1)\exp[j(\tau_x x_1 + \tau_y y_1)], \quad (5)$$

where x_1 and y_1 are the spatial coordinates shown in Figure 1, $d(x_1, y_1)$ is the Fourier transform of the polarized modal electric field; τ_x and τ_y are linear tilt constants in the horizontal and vertical directions, respectively.

Following this, the phase of the complex field, $f(x_1,y_1) = u(x_1,y_1) + jv(x_1,y_1)$, is binarized according to the amplitude mapping shown in Figure 3, adapted from [9]. The binarized modal field is then displayed on the SLM. The binarized waveform may be expressed as a series of harmonics in a Fourier series expansion (Figure 4):

$$g(x_1, y_1) = a_o + \frac{4}{\pi}\sum_{n=1}^{\infty} a_n \cos\{n[\xi(x_1, y_1) + \tau_x x_1 + \tau_y y_1]\}, \quad (6)$$

where $a_o = 2\alpha(x_1, y_1)/\pi - 1$ is the constant term and $a_n = \sin[n\alpha(x_1, y_1)]/n$ is the Fourier cosine coefficient of the Fourier series expansion. $L1$ then takes the Fourier transform of the binarized modal field on the SLM. Taking the Fourier transform of Equation (6) yields:

$$G(x_2, y_2) = M_o(x_2, y_2) + \sum_{n=1}^{\infty}\left[M_n(x_2 + n\tau_x, y_2 + n\tau_y) + M_n^*(n\tau_x - x_2, n\tau_y - y_2)\right], \quad (7)$$

where x_2 and y_2 are the spatial coordinates in the Fourier plane of the lens, * is the complex conjugate and $M_n(x_1, y_1)$ is the nth diffraction order, given by:

$$M_n(x_1, y_1) = \mathcal{F}\{a_n(x, y)\} = \mathcal{F}\{\sin[n\alpha(x_1, y_1)]\}/n. \quad (8)$$

The effect of the tilt is to separate the diffraction orders by multiples of the tilt constants in the Fourier plane. The first diffraction order, M_1, is then spatially filtered by coupling it carefully into the MMF.

Taking the inverse Fourier transform of M_1 yields the original polarized transverse electric field for LP_{lm}, $b(x, y)$:

$$\mathcal{F}^{-1}\{M_1(x, y)\} = b(x, y). \quad (9)$$

where $\mathcal{F}^{-1}$ is the inverse Fourier transform operator.

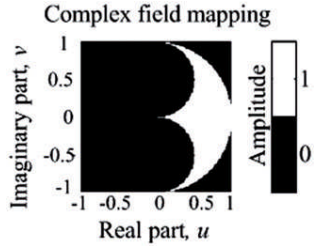

Figure 3. The mapping of a complex field onto the required amplitude (from [9]). Reproduced with permission from Neil et al. J. Microsc. 2000, 197, 219–223. Copyright (2000) by John Wiley and Sons. (The color version of this figure is included in the online version of the journal.)

3. Simulation of binary amplitude-modulated SLM holograms

The binary-amplitude spatially modulated SLM hologram for the desired mode was simulated using MATLAB [11]. The steps are described as follows. First, a linearly polarized modal electric field of the desired mode is simulated. The array of the original polarized modal field for the desired mode is given by:

$$b(i, j), \quad 0 \le i \le 127, \; 0 \le j \le 127, \quad (10)$$

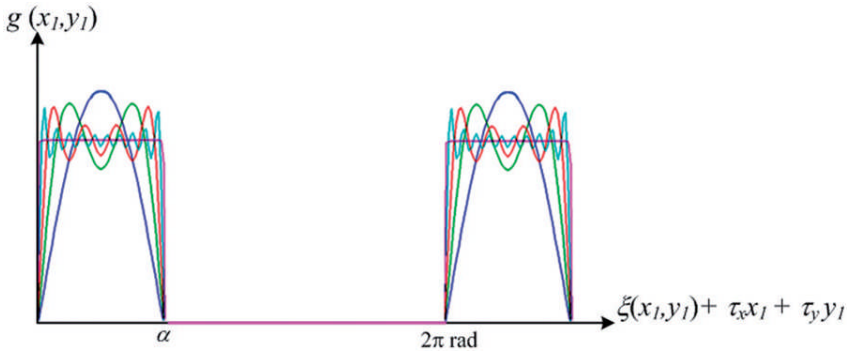

Figure 4. The binarized waveform expressed as a Fourier series. (The color version of this figure is included in the online version of the journal.)

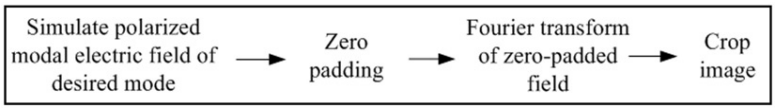

Figure 5. Steps for obtaining the Fourier transform of the modal electric field.

where i and j are pixel numbers in the horizontal and vertical directions, respectively, in the plane of the original modal electric field.

The next step in the simulation of the SLM hologram is to take the Fourier transform of the polarized modal electric field of the desired mode. The steps for obtaining the Fourier transform of the polarized modal electric field are summarized in Figure 5. MATLAB performs the two-dimensional discrete Fourier transform of $c(i, j)$ using a fast Fourier transform (FFT) algorithm. In the FFT, the number of sample points in the Fourier plane is fixed.

To increase the resolution of the image in the Fourier plane, the number of sample points in the plane of the original modal electric field must be increased. This may be done by acquiring more samples in the original plane, which may be computationally expensive. Alternatively, the number of samples in the original plane may be increased by preserving the original modal electric field but appending zeros to the original modal electric field array before the Fourier transform. This is also known as zero-padding. Before taking the Fourier transform of the modal electric field of the desired mode, the original 128×128 pixel modal electric field array, $c(i,j)$, was zero-padded to form a 480×480 pixel array. The zero-padded modal electric field, $c_{pad}(i, j)$, may be written as:

$$c_{pad}(i,j) = \begin{cases} c(i,j), & 0 \le i \le 127,\ 0 \le j \le 127 \\ 0, & 128 \le i \le 479,\ 128 \le j \le 479 \end{cases} \tag{11}$$

where i and j are pixel numbers in the horizontal and vertical directions, respectively, in the plane of the original modal electric field. Then, applying a Fourier transform to the zero-padded modal electric field, $c_{pad}(i,j)$, the following is obtained:

$$\begin{aligned} C_{pad}(p,q) = &\sum_{i=0}^{127}\sum_{j=0}^{127} c(i,j)\exp(-j2\pi ip/479) \\ &\exp(-j2\pi iq/479) \\ &+ \sum_{i=128}^{479}\sum_{j=128}^{479} 0\cdot\exp(-j2\pi ip/479) \\ &\exp(-j2\pi jq/479) \end{aligned} \tag{12}$$

where p and q are pixel numbers in the horizontal and vertical directions, respectively, in the Fourier plane. Equation (12) shows that the effect of the zero-padding was to evaluate $C_{pad}(p,q)$ at 480 uniformly-spaced pixels across one period of 2π instead of only 128 uniformly-spaced pixels without zero-padding. Thus, $C_{pad}(p,q)$ was sampled at smaller spatial frequency intervals, increasing the discernibility of fine details in $C_{pad}(p,q)$. $C_{pad}(p,q)$ is an array of 480×480 pixels, given as:

$$C_{pad}(p,q), \quad 0 \le p \le 479,\ 0 \le q \le 479. \tag{13}$$

Next, the center of the 480×480 pixel $C_{pad}(p,q)$ was cropped to an array of 128×128 pixels. This new array, $S(p,q)$, which is a subset of $C_{pad}(p,q)$, may be written as:

$$S(p,q) = C_{pad}(p,q), \quad 177 \le p \le 304,\ 177 \le q \le 304. \tag{14}$$

The reason for selecting an array of 480×480 pixels for the Fourier plane in the zero-padding process was to ensure that the area containing the modal field pattern within the Fourier plane neither exceeded the center 128×128 pixels of $C_{pad}(p,q)$ nor under-utilized the center 128×128 pixels. This was to ensure that the 128×128 pixels of the active area of the SLM were efficiently utilized. Using a Fourier plane array of 480×480 pixels and cropping the center 128×128 pixels, the modes span between 35.2% and 88.3% of the total active area of the SLM.

The parameters used for the simulation of the Fourier transform of the modal field of the MMF are shown in Table 1. Typical Fourier transforms of the modal field are shown in Figure 6.

The third step in the simulation of the SLM hologram is to add linear tilt constants to (p,q) in both the x and y directions, following the approach in [9], as described mathematically in Equation (5). Linear tilt constants $\tau_x = 88\pi$ in the horizontal direction and $\tau_y = 1208\pi$ in the vertical direction, as in [9], provided sufficient separation of the diffraction orders in the Fourier plane, hence facilitated the isolation of the first diffraction order.

Finally, the tilted field was then binarized according to the phase mapping scheme shown in Figure 3.

Table 1. Parameters used for simulation of modal field patterns.

Parameters for simulation	Value
Core radius, r	31.25 μm
Wavelength in free space, λ	632.8 nm
Numerical aperture, NA	0.275
Normalized frequency, $V = 2\pi rNA/\lambda$	85.3289

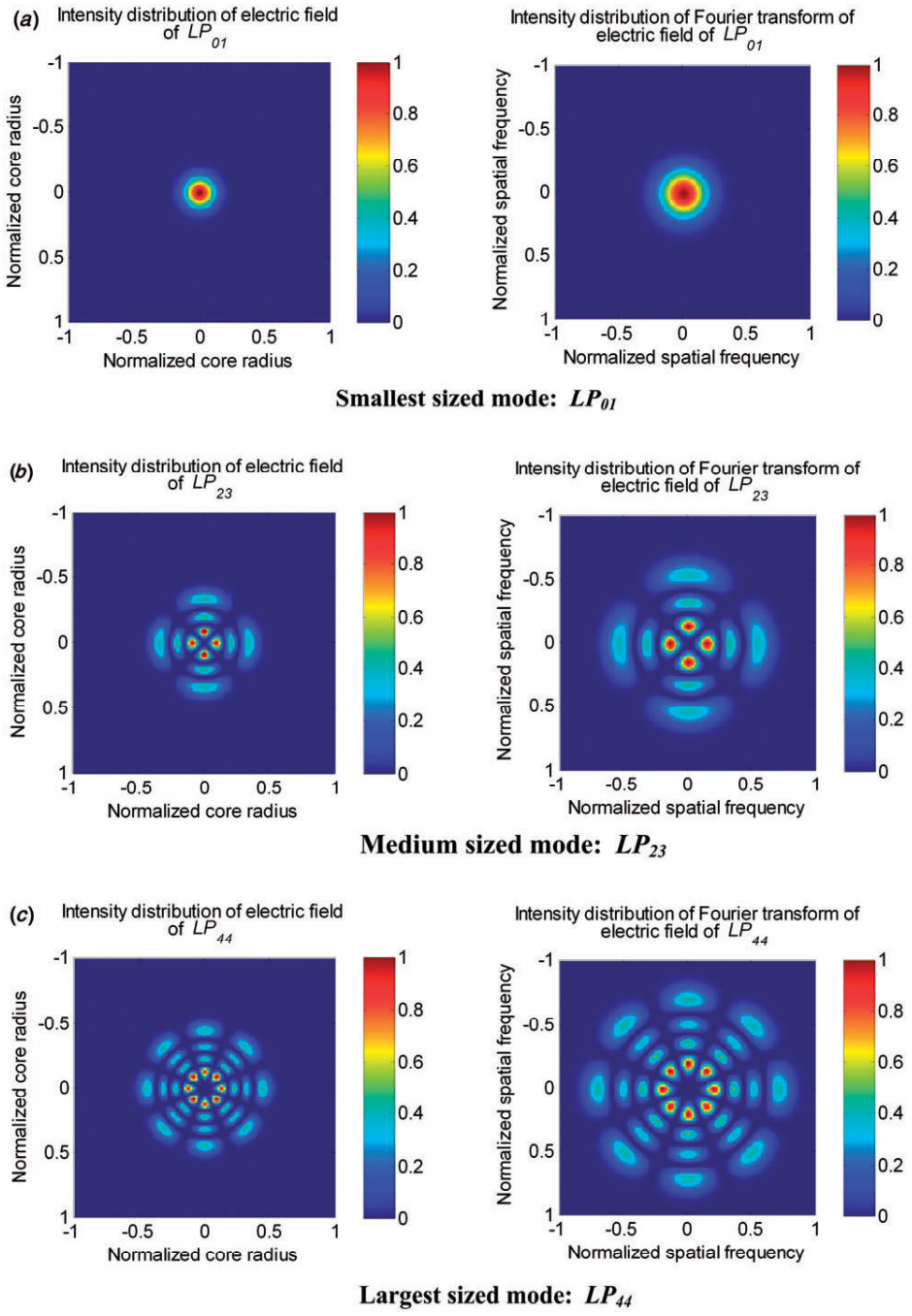

Figure 6. Intensity distribution of modal electric fields and their corresponding Fourier transforms. (*a*) For LP_{01}, the Fourier transformed mode spans 35.2% of the SLM active area. (*b*) For LP_{23}, the Fourier transformed mode spans 72.7% of the SLM active area. (*c*) For LP_{44}, the Fourier transformed mode spans 88.3% of the SLM active area. (The color version of this figure is included in the online version of the journal.)

Figure 7 illustrates typical Fourier transformed field patterns and the corresponding binarized patterns for the SLM. MATLAB and Labview were used for converting the SLM pattern to the correct format and for displaying it on the SLM.

4. Application of new binary spatial amplitude modulation scheme

This section provides an application of the new binary spatial amplitude modulation scheme for mode selectivity in optical fiber communications. Mode selectivity

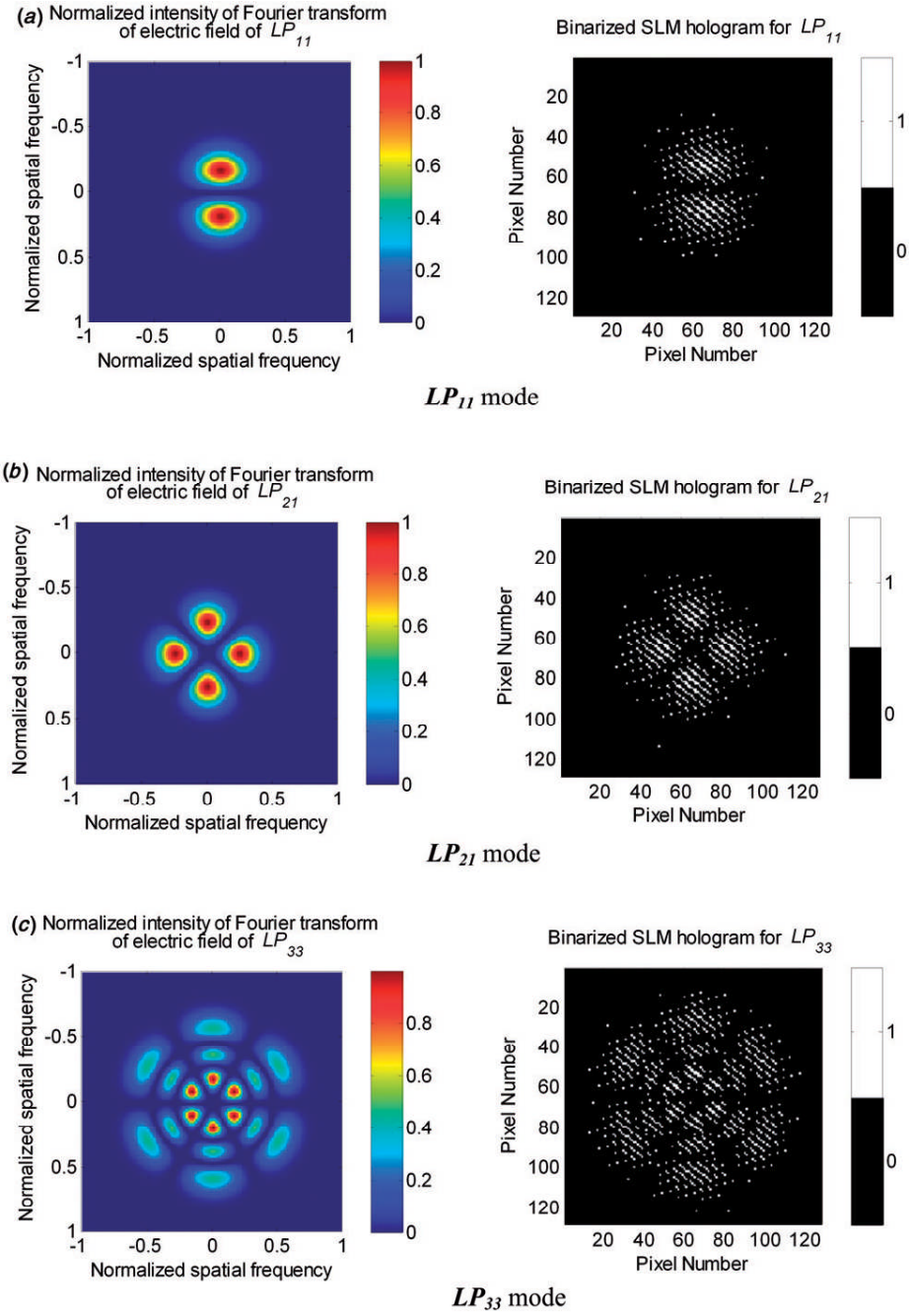

Figure 7. Fourier transform of modal fields and their corresponding binarized SLM holograms using tilt constants $\tau_x = 88\pi$ in the horizontal direction and $\tau_y = 120\pi$ in the vertical direction. For the binarized SLM holograms, 1 indicates intensity transmission and 0 indicates no intensity transmission. The total number of pixels of the SLM area is 128×128 pixels. The pixel number on the vertical axis starts from the top of SLM active area, while on the horizontal axis, the pixel number starts from the left-most of the SLM active area. (The color version of this figure is included in the online version of the journal.)

is the accuracy in filtering the desired mode or mode group from other propagating modes within the waveguide or optical fiber. Mode selectivity generally depends on the power coupling of the incident electric field into the modal field of the desired mode, as well as the number of modes or mode groups excited per launch. In optical fiber communications, mode selectivity facilitates strategic enhancement of desirable features such as reduced dispersion [12–22], enhanced channel bandwidth by spatial multiplexing [23–28] or reduced error in the signal detection by to increasing the number of redundant channels [12,29–31]. In local area network multimode fiber backbones, this is crucial as the rapidly increasing demands for higher bandwidth may soon overwhelm the current network infrastructure [32–34]. As a motivation for the use of the new modulation scheme described in Section 2, the new binary spatial amplitude modulation scheme was used by a transmissive binary spatial light modulator in a mode selectivity experiment. The experimental setup is shown Figure 1. In this mode selectivity experiment, any desired LP_{lm} mode comprising any azimuthal mode number l and any radial mode number m could be selected. The new modulation technique was tested on all LP modes from LP_{01} to LP_{44}. As an example, the electric field for the LP_{41} mode was generated. An array of the binary amplitude-modulated modal electric field was calculated based on the technique described in Section 3 and was displayed on a transmissive binary amplitude SLM with an active area of 8 mm, as shown in Figure 8(*a*). The binary amplitude spatially modulated modal electric field was then Fourier transformed by the lens. The Fourier plane of $L1$ from the experiment was then measured, as shown in Figure 8(*c*). As a reference, the Fourier plane was simulated using MATLAB, as shown in Figure 8(*b*). It was observed that the measured Fourier plane of $L1$ (Figure 8(*c*)) is in good agreement with the simulated Fourier plane of $L1$ (Figure 8(*b*)). The extent of the zero order Fourier plane was calculated using [35]:

$$\text{Width of zero order Fourier plane} = \lambda f/\Delta_h, \qquad (15)$$

where λ is the wavelength of the illuminating beam, f is the focal length of the lens and Δ_h is the hologram plane sampling period. Substituting $\lambda = 632.8$ nm, $f = 75$ mm and $\Delta_h = 78.125$ μm into Equation (15), the width of the zeroth order Fourier plane was calculated to be 607.5 μm. Having established the extent of the zeroth order Fourier plane, the first diffraction order was identified. The first diffraction order was then isolated using a pinhole and coupled into the multimode fiber.

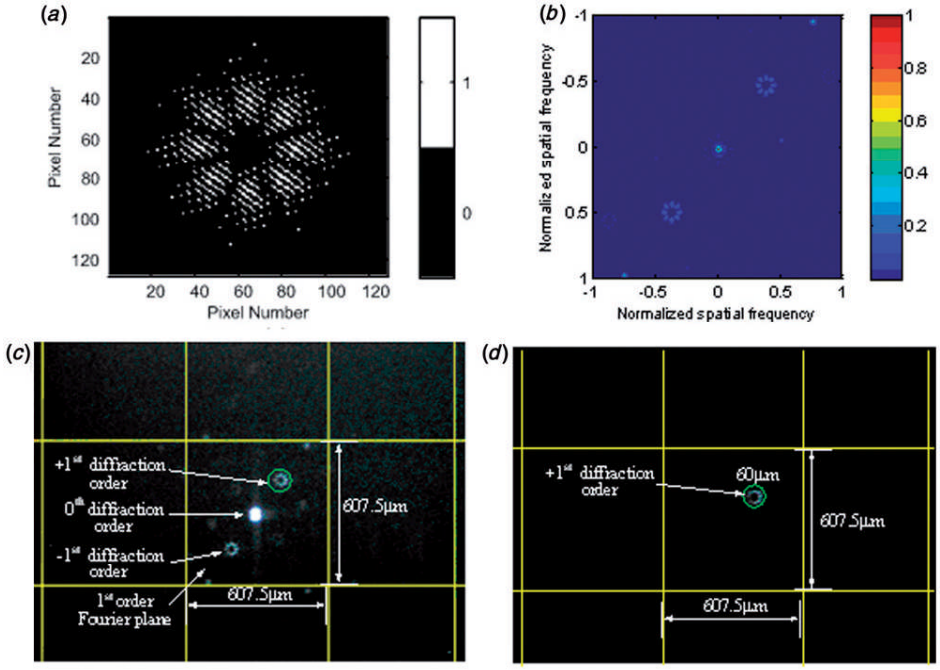

Figure 8. (*a*) SLM hologram for LP_{41} mode. (*b*) Simulated intensity distribution of Fourier plane of *L1* for LP_{41} mode. (*c*) Measured intensity distribution of Fourier plane of *L1* for LP_{41} mode and location of first diffraction order. (*d*) Isolation of first diffraction order for LP_{41} mode using pinhole for validation. (The color version of this figure is included in the online version of the journal.)

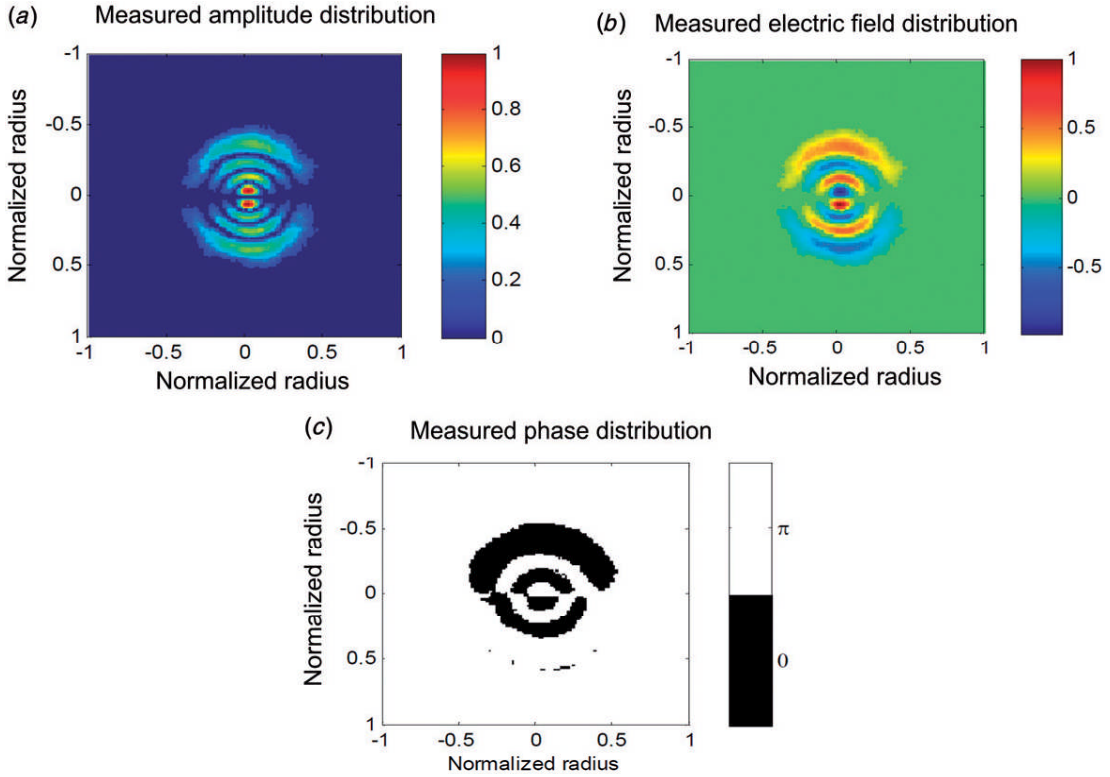

Figure 9. Combination of amplitude and phase distributions of generated modal field to obtain the modal electric field for LP_{14} ($F_{lm}\cos l\phi$ polarization). (The color version of this figure is included in the online version of the journal.)

Before displaying the image at the input endface of the multimode fiber, the new binary amplitude spatial modulation technique was verified. This is discussed in the next section.

5. Verification of new binary spatial amplitude modulation scheme

For verification of the new binary spatial amplitude modulation scheme, a 60 μm pinhole was placed in the Fourier plane of the lens to extract the first diffraction order. As an example, the first diffraction order on the Fourier plane for the LP_{41} mode was extracted, as shown in Figure 8(*d*). The extracted first diffraction order was then measured. An example of the measured amplitude and phase distributions of generated modal field to obtain the complete modal electric field distribution is shown in Figure 9.

The power coupling efficiency of the generated modal field was calculated using:

$$\eta_{l,m} = \left|\iint_{A_{core}} \mathbf{E}_{in}(x,y)\mathbf{e}^{*}_{l,m}(x,y)\mathrm{d}x\mathrm{d}y\right|^2 \Big/ \iint_{A_{core}} \left|\mathbf{E}_{in}(x,y)\right|^2\mathrm{d}x\mathrm{d}y \iint_{A_{core}} \left|\mathbf{e}_{l,m}(x,y)\right|^2\mathrm{d}x\mathrm{d}y, \quad (16)$$

where e_{lm} is the image of the measured generated modal electric field extracted by the pinhole and elm is the image of theoretical modal electric field for the LP_{lm} mode given in [10]. Substituting $\mathbf{E}_{in}$ and e_{lm} for the desired mode into Equation (16), the power coupling efficiency of the various generated modal fields compared to theoretical modes were calculated. The power coupling efficiencies of the generated modal electric fields are shown in Figure 10. The power coupling efficiencies of the generated modal electric fields with respect to the theoretical mode are in the range of 92.5% to 97.2%, after equalizing the image size and orientation of the images of both electric fields.

Thus, the generated modal electric field is a close approximate of the theoretical modal electric field. This implies that approximately 92.5% to 97.2% of the generated modal electric would be coupled into the MMF at the input, assuming no insertion losses. Thus, this shows that the retrieved electric field is in good agreement with the original modal electric field transmitted and verifies the new binary amplitude-modulated technique using a single lens. The experiment in Section 4 was repeated three times for each LP mode within the range of $l = 0, 1, \ldots, 4$ and $m = 1, 2, \ldots, .4$ and the difference between the readings

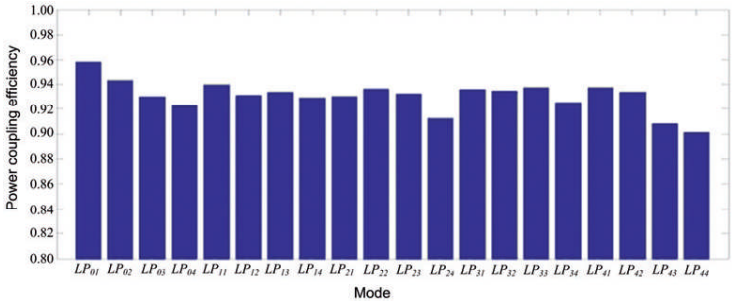

Figure 10. Power coupling efficiency of generated modal field with respect to theoretical modal field. (The color version of this figure is included in the online version of the journal.)

for each mode was within 0.5%. The discrepancy between the generated modal electric field and the theoretical modal electric field is due to spherical aberration, caused by to the orientation of the lens and the large reduction of the size of the electric field from the input to the optical fiber.

6. Conclusions

A new amplitude modulation technique for mode selectivity in optical fiber using a single lens is demonstrated. The continuous transverse modal electric field of an infinite parabolic multimode fiber is modulated by two amplitude levels. The new modulation scheme is applied in an optical fiber communications for mode selectivity. Results show that the retrieved electric field is in good agreement with the original modal electric field transmitted.

Acknowledgements

The author would like to thank Dr Dominic O'Brien, Dr Frank Payne, Dr Martin Booth and Grahame Faulkner at the University of Oxford for their valuable advice and important feedback.

References

[1] Peters, K. *Smart Mater. Struct.* **2011,** *20,* 1–17.
[2] Su, H.; Zervas, M.; Furlong, C.; Fischer, G.S. *MEMS Nanotechnol.* **2011,** *4,* 131–136.
[3] Cortez-Retamozo, V.; Swirski, F.K.; Waterman, P.; Yuan, H.; Figueiredo, J.L.; Newton, A.P.; Upadhyay, R.; Vinegoni, C.; Kohler, R.; Blois, J.; Smith, A.; Nahrendorf, M.; Josephson, L.; Weissleder, R.; Pittet, M.J. *J. Clin. Invest.* **2008,** *118,* 4058–4066.
[4] Sibillano, T.; Ancona, A.; Berardi, V.; Lugarà, P.M. *Sensors* **2009,** *9,* 3376–3385.
[5] Kaneda, N.; Yang, Q.; Liu, X.; Chandrasekhar, S.; Shieh, W.; Chen, Y.-K. *J. Lightwave Technol.* **2010,** *28,* 494–501.
[6] Ip, E.M.; Kahn, J.M. *J. Lightwave Technol.* **2010,** *28,* 502–519.
[7] Spinnler, B. *IEEE J. Sel. Top. Quantum Electron.* **2010,** *16,* 1180–1192.
[8] Leven, A.; Kaneda, N.; Corteselli, S. *IEEE J. Sel. Top. Quantum Electron* **2010,** *16,* 1227–1234.
[9] Neil, M.A.A.; Wilson, T.; Juskaitis, R. *J. Microsc.* **2000,** *197,* 219–223,.
[10] Snyder, A.W.; Love, J.D. *Optical Waveguide Theory*; Chapman and Hall: London, 1983.
[11] MATLAB, version 7.8.0.347; the language of technical computing R2009a; Mathworks, 2009.
[12] Alon, E.; Stojanovic, V.; Kahn, J.M.; Boyd, S.; Horowitz, M. In *Proceedings of GLOBECOM '04, the IEEE Global Telecommunications Conference*, Dallas, TX, November 29–December 3, 2004; pp 1023–1029.
[13] Neo, P.L.; Freeman, J.P.; Wilkinson, T.D. Presented at the Optical Fiber Communication (OFC) and the National Fiber Optic Engineers Conference (NFOEC), March 25–29, 2007, California, USA.
[14] Amphawan, A. *Opt. Express* **2011,** *19,* 9056–9065.
[15] Panicker, R.A.; Kahn, J.M. *J. Lightwave Technol.* **2009,** *27,* 5790–5799.
[16] Panicker, R.A.; Kahn, J.M.; Boyd, S.P. *J. Lightwave Technol.* **2008,** *26,* 1295–1303.
[17] Panicker, R.A.; Lau, A.P.T.; Wilde, J.P.; Kahn, J.M. *J. Lightwave Technol.* **2009,** *27,* 5783–5788.
[18] Shemirani, M.B.; Kahn, J.M. *J. Lightwave Technol.* **2010,** *28,* 2084–2095.
[19] Shen, X.; Kahn, J.M.; Horowitz, M.A. *Opt. Lett.* **2005,** *30,* 2985–2987.
[20] Amphawan, A.; Payne, F.; O'Brien, D.; Shah, N. *J. Lightwave Technol.* **2010,** *28,* 861–869.
[21] Raddatz, L.; White, I.H.; Cunningham, D.G.; Nowell, M.C. *J. Lightwave Technol.* **1998,** *16,* 324–331.
[22] Siuzdak, J.; Nowak, R.; Stepniak, G. *WSEAS Trans Commun.* **2005,** *4,* 299–305.
[23] Jalali, B.; Hsu, R.C.J.; Shah, A.R. *Coherent Optical MIMO*; SPIE: Bellingham, WA, 2005; pp 121–127.

[24] Stuart, H.R. *Science* **2000,** *289,* 281–283.
[25] Salsi, M.; Koebele, C.; Sperti, D.; Tran, P.; Brindel, P.; Mardoyan, H.; Bigo, S.; Boutin, A.; Verluise, F.; Sillard, P.; Astruc, M.; Provost, L.; Cerou, F.; Charlet, G. Presented at the Optical Fiber Communication Conference and Exposition (OFC) and the National Fiber Optic Engineers Conference (NFOEC) 2011, Los Angeles, CA, March 6–10, 2011.
[26] Li, A.; Amin, A.A.; Chen, X.; Shieh, W. Presented at the Optical Fiber Communication Conference and Exposition (OFC) and the National Fiber Optic Engineers Conference (NFOEC) 2011, Los Angeles, CA, March 6–10, 2011.
[27] Ryf, R.; Randel, S.; Gnauck, A.H.; Bolle, C.; Essiambre, R.-J.; Winzer, P.J.; Peckham, D.W.; McCurdy, A.; Lingle, J.R. Presented at the Optical Fiber Communication Conference and Exposition (OFC) and the National Fiber Optic Engineers Conference (NFOEC) 2011, Los Angeles, CA, March 6–10, 2011.
[28] Hanzawa, N.; Saitoh, K.; Sakamoto, T.; Matsui, T.; Tomita, S.; Koshiba, M. Presented at the Optical Fiber Communication Conference and Exposition (OFC) and the National Fiber Optic Engineers Conference (NFOEC) 2011, Los Angeles, CA, March 6–10, 2011.
[29] Patel, K.M. *IEEE Photonics Technol. Lett*. **2002,** *14,* 393–395.
[30] Lenz, D.; Rankov, B.; Erni, D.; Bächtold, W.; Wittneben, A. In *Proceedings of the International Zurich Seminar on Communications (IZS)*, 2004; pp 196–199.
[31] Erni, D.; Jungo, M.; Baechtol, W. In *Proceedings of the Workshop on Compound Semiconductor Devices and Integrated Circuits (WOCSDICE)*, 2003; pp 67–68.
[32] Cisco, *Hyperconnectivity and the Approaching Zettabyte Era;* 2010.
[33] Stepniak, G.; Maksymiuk, L.; Siuzdak, J. Presented at the 36th European Conference on Optical Communications, Turin, Italy, September 19–23, 2010.
[34] Xirasagar, S. *Next Generation Networks (NGN)* **2010,** *2*. http://www.tmcnet.com/ngnmag/0110/traffic-management-for-emerging-networks.htm
[35] O'Brien, D. Dynamic Holograms for Optical Interconnection. Ph.D. Thesis, Cambridge University, 1993.